catalysts

MDPI

Article

Activated Carbon-Supported Tetrapropylammonium Perruthenate Catalysts for Acetylene Hydrochlorination

Xing Li [1,2], Haiyang Zhang [1,2,*], Baochang Man [1,2], Lijuan Hou [1,2], Chuanming Zhang [1,2], Hui Dai [3], Mingyuan Zhu [1,2], Bin Dai [1,2], Yanzhao Dong [3] and Jinli Zhang [1,3,*]

1 School of Chemistry and Chemical Engineering of Shihezi University, Shihezi 832000, China; 18299388851@139.com (X.L.); 13070097209@163.com (B.M.); 18205482907@163.com (L.H.); zhchming163@163.com (C.Z.); zhuminyuan@shzu.edu.cn (M.Z.); db_tea@shzu.edu.cn (B.D.)

2 Key Laboratory for Green Processing of Chemical Engineering of Xinjiang Bingtuan, Shihezi 832000, China

3 School of Chemical Engineering & Technology, Tianjin University, Tianjin 300072, China; daihui028@tju.edu.cn (H.D.); yzdong@tju.edu.cn (Y.D.)

* Correspondence: zhy198722@163.com (H.Z.); zhangjinli@tju.edu.cn (J.Z.); Tel.: +86-99-3205-7277 (H.Z.); +86-22-2789-0643 (J.Z.); Fax: +86-99-3205-7210 (H.Z.); +86-22-2740-3389 (J.Z.)

Received: 13 October 2017; Accepted: 20 October 2017; Published: 24 October 2017

Abstract: The Ru-based catalysts, including Ru/AC (activated carbon), TPAP (tetrapropylammonium perruthenate)/AC, TPAP/AC-HNO_3, and TPAP/AC-HCl, were prepared and assessed for the direct synthesis of vinyl chloride monomer. The results indicate that the TPAP/AC-HCl catalyst exhibits the best performance with the conversion falling from 97% to 91% in 48 hours' reaction under the conditions of 180 °C, a GHSV(C_2H_2) of 180 h^{-1}, and the feed ratio V_{HCl}/V_{C2H2} of 1.15. The substitution of $RuCl_3$ precursor with high valent TPAP species leads to more ruthenium oxides active species in the catalysts; the acidification treatment of carrier in TPAP/AC catalyst can produce an enhanced interaction between the active species and the modified functional groups on the carrier, and it is beneficial to inhibit the carbon deposition and sintering of ruthenium species in the reaction process, greatly increase the adsorption ability of reactants, and further increase the amount of dominating active species in the catalysts, thus improving the catalytic performance. This also provides a promising strategy to explore high efficient and economic mercury-free catalysts for the hydrochlorination of acetylene.

Keywords: tetrapropylammonium perruthenate; acetylene hydrochlorination; Ru catalysts

1. Introduction

Although the addition reaction of acetylene with hydrogen chloride is an essential route for the direct synthesis of vinyl chloride monomer (VCM), the catalyst ever used in traditional industry is carbon-supported $HgCl_2$, which posseses a serious environmental pollution and personnel hazard for its high toxicity and effumability. Hg resources are in short supply, and an excess of 140 countries have reached an agreement about the "Minamata Convention on Mercury" in the year 2013, appealing to the people around the world to eliminate the processes using mercury or mercury compounds as the catalysts to produce VCM. According to the new laws, the current $HgCl_2$-based catalyst must be substituted by mercury-free catalysts before 2022. In recent years, the research of non-mercury catalysts has always been a focus.

Hutchings et al. were the first to show that the catalytic ability of metal catalysts is linked to the electrode potential of the associated metal ions, and the supported catalysts, whose metal species possessed the higher standard electrode potentials, exhibited the higher activities [1]. In addition,

the reverse electronic effects may also be used to accomplish the reaction [2]. Accordingly, the gold based catalysts were most active for the direct synthesis of VCM [3–8]. However, the high cost of the initial investment restricts the scope of the Au-based catalysts' industrial application. The high valent ruthenium oxides also possess higher standard electrode potentials, and Zhu et al. found that the calculated activation barrier of $RuCl_3$, $AuCl_3$, and $HgCl_2$ catalysts is 9.1, 11.9, and 16.3 kcal mol^{-1}, respectively [9]. Therefore, $RuCl_3$ may be one of the probable substitute catalysts for acetylene hydrochlorination. Whereafter, extensive researches on the Ru-based catalysts have been carried out, for example, Li et al. came to a conclusion that Ru catalysts deposited inside carbon nanotubes exhibits better catalytic performance, with a 95.0% conversion and a 99.9% selectivity to VCM at 170 °C, the feed ratio V_{HCl}/V_{C2H2} of 1.10, and a C_2H_2 gas hourly space velocity (GHSV) of 90 h^{-1} [10]. Gu et al. reported that complexes like ammonium hexachlororuthenate performs a higher catalytic performance for the synthesis of VCM with a 90% conversion and a 99.6% selectivity to VCM at 170 °C, $V_{(HCl)}/V_{(C2H2)}$ of 1.1 and a GHSV(C_2H_2) of 180 h^{-1} [11]. Zhang et al. reported that the conversion continues to be above 95% within 48 h over the Ru1Co3/SAC catalyst under the conditions of 170 °C, V_{HCl}/V_{C2H2} of 1.1 and a GHSV(C_2H_2) of 180 h^{-1} [12]; it is illustrated that the doped cobalt metal affected to a large extent the amount of ruthenium species (RuO_x, RuO_2, $RuCl_3$, and Ru^0) in the catalyst, resulting in the good ability to inhibit the coke deposition of the catalyst. Shang et al. reported that the synthesized 1%Ru@15%TPPB/AC catalyst exhibited a 99.7% conversion and a 99.9% selectivity to VCM after 48 h under the conditions of 170 °C, V_{HCl}/V_{C2H2} of 1.15 and a GHSV(C_2H_2) of 360 h^{-1} [13]. Man et al. discovered that the oxidation modification boosted the reciprocity between the Ru species and oxygenated functional groups, which could enhance the catalysts' activity and the modified Ru-O/AC-O exhibited an excellent performance, with a 99.6% initial C_2H_2 conversion of at 180 °C, V_{HCl}/V_{C2H2} of 1.15 and a GHSV(C_2H_2) of 180 h^{-1} [14].

Nanostructured supports, such as Al_2O_3 [15], metal organic frameworks (MOFs)-derived solid bases [16], mesoporous silica nanoparticles (MSNs) [17], metal oxide supports (MO_x) [18], etc., are usually used for the catalytic reaction. However, due to the different physicochemical properties, some of them are not beneficial to act as an effective support for acetylene hydrochlorination. Benefiting from the developed pore structure and interactive functions at the surface, activated carbon (AC) becomes an ideal support in the reaction of acetylene hydrochlorination [19]. According to previous reports, functional groups on the carrier surface can influence the properties of active species. For example, Zhao et al. demonstrates that the synergistic effect between nitrogen and ruthenium can effectively promote the catalytic activity of the prepared catalyst in the dehydrochlorination of 1,2-dichloroethane to synthesize VCM [20], Xu et al. improved obviously the catalytic activity of Ru-based catalyst via adding N-containing groups to the activated carbon carrier, strikingly, $–NH_2$ contributed to the optimal catalytic performance of Ru-based catalyst with a 93.2% conversion and a 99.0% selectivity to VCM under the conditions of 180 °C, a V_{HCl}/V_{C2H2} of 1.15 and a GHSV(C_2H_2) of 360 h^{-1}, and there is no obvious decline within 48 h [21].

According to the understanding of previous works, high valent ruthenium species are the key active species in the Ru catalysts for acetylene hydrochlorination. High valent ruthenium species were usually obtained through the modification of $RuCl_3$ or the carries, and there are few literatures related to the applications of ruthenium complexes catalysts with high valent ruthenium species for acetylene hydrochlorination. As a consequence, we prepared the Ru-based catalysts with the tetrapropylammonium perruthenate (TPAP) supported on AC, which was treated by a certain concentration of hydrochloric acid or nitric acid in this paper, and evaluated the catalytic performannce for the hydrochlorination of acetylene, intending to find out an easily prepared, higher activated, more stable and economic mercury-free catalyst. The effect of the supported ruthenium complexes catalysts on the catalytic behavior was also explored in detail.

2. Results and Discussion

2.1. Performance Test Results of the Prepared Catalysts

All of the prepared catalysts were assessed for the direct synthesis of VCM, and the VCM synthesis results for the prepared catalysts are shown in Figure 1. The bare AC, AC-HNO_3, and AC-HCl show relatively lower activity for the hydrochlorination reaction of acetylene with acetylene conversions of 7.1%, 5.7%, and 6.4%, respectively (Figure 1a). The original Ru/AC catalyst has a 48.3% conversion at 48 h. When compared with the original Ru/AC, the activity of TPAP/AC catalyst is greatly improved. The acidification modification of AC is also beneficial for the Ru catalysts to catalyze the reaction, a 84.8% acetylene conversion can be yielded over the TPAP/AC-HNO_3 catalyst, and the best catalytic activity can be achieved over TPAP/AC-HCl catalyst with a stable acetylene conversion of 89.8% within 48 hours' reaction. All of the related catalysts exhibit more than 99% selectivity to VCM during the reaction (Figure 1b). The results show that the pretreatment of activated carbon, especially the acidification modification by hydrochloric acid, may produce an interaction between the actives species and the carrier, which significantly promotes the catalytic performance of the prepared catalysts for the direct synthesis of VCM.

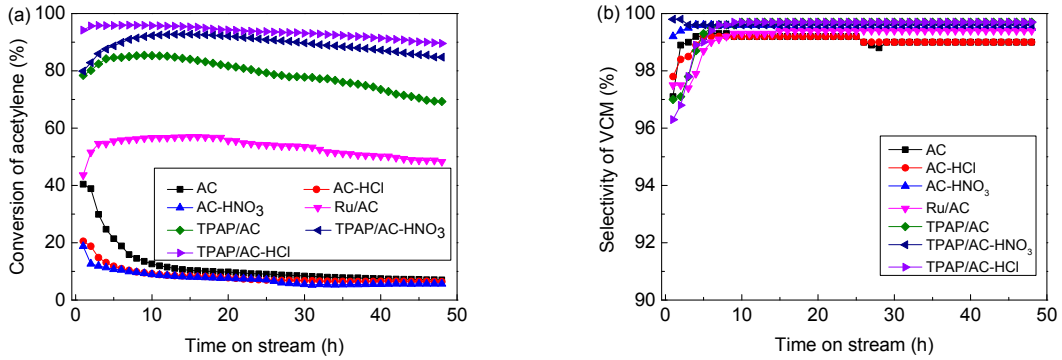

Figure 1. Acetylene conversion (**a**) and selectivity to vinyl chloride monomer (VCM) (**b**) over the prepared catalysts. Reaction conditions: temperature (T) = 180 °C, GHSV(C_2H_2) = 180 h^{-1}, and V_{HCl}/V_{C2H2} = 1.15.

2.2. Catalyst Characterization

To reveal the physicochemical properties of the Ru-based catalysts, several characterization techniques were conducted, and the results are discussed as below.

2.2.1. The Functional Groups on the Catalysts' Surface

The Fourier transform infrared spectra (FT-IR) spectra of the prepared catalysts were recorded to reflect the functional groups on the prepared catalysts' surface. The characteristic bands of the fresh bare AC, AC-HNO_3, AC-HCl, pure TPAP, original Ru/AC, TPAP/AC-HCl, and TPAP/AC-HNO_3 catalysts are shown in Figure 2. There are several characteristic peaks appear at 1091, 1384, 2350, and 3400 cm^{-1} for the fresh bare AC, related to the C–OH, C=O, C≡N, and phenolic hydroxyl stretching vibration bands, respectively [22–24]. Mealwhile, the peak intensity of C≡N and phenolic hydroxyl stretching vibration bands in AC-HNO_3 catalysts is further enhanced, while that of C–OH band is weakened as compared with the fresh bare AC. However, the peak intensity of C–OH, C=O and phenolic hydroxyl stretching vibration bands in AC-HCl catalysts is reduced, while that of C≡N stretching vibration band is reinforced after the treatment by hydrochloric acid, demonstrating that the functional groups were modified to a certain extent by acidification on the AC surface. It can improve the hydrophilicity of the carrier, thus improving the dispersion of active species on the surface. As for the original Ru/AC catalyst, the intensity of C≡N stretching vibration band, as well as the oxygen-containing functional groups, decreased to different degrees. For the TPAP/AC, the intensity

of C≡N stretching vibration band is lower than that of the original Ru/AC catalyst, however, the intensity of phenolic hydroxyl stretching vibration band is higher than that of the original Ru/AC catalyst. Additionally, the characteristic bands of TPAP also appear at 1070 cm^{-1} and 1400 cm^{-1}. When compared with TPAP/AC, TPAP/AC-HNO_3, and TPAP/AC-HCl show characteristic peaks at 1070 cm^{-1} and 1400 cm^{-1} and 2969 cm^{-1}, respectively, corresponding to the basic vibration bands of C–N, –CH_3, and –C–H groups [25–27]. When TPAP (Scheme 1) is loaded on the activated carbon pretreated by nitric acid, the above characteristic peaks disappeared. It should be noted that some functional groups, especially the C≡N stretching vibration bands, have a slight red-shift, which may be due to the interaction between the ruthenium specie in TPAP and the functional groups on the surface of AC.

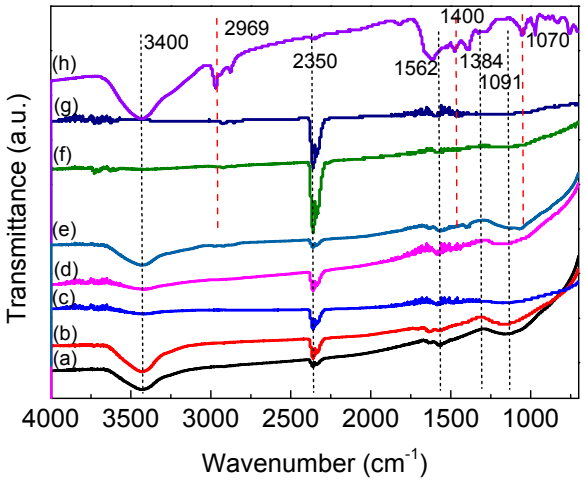

Figure 2. Fourier transform infrared spectra (FT-IR) spectra of (**a**) AC, (**b**) AC-HNO_3, (**c**) AC-HCl, (**d**) Ru/AC, (**e**) TPAP/AC, (**f**) TPAP/AC-HNO_3, (**g**) TPAP/AC-HCl, (**h**) TPAP. The characteristic peaks are centered at: 1091 cm^{-1}: C–OH; 1384 cm^{-1}: C=O; 1562 cm^{-1}: COOH; 2350 cm^{-1}: C≡N; 3400 cm^{-1}: phenolic hydroxyl; 1070 cm^{-1}: C–N; 1400 cm^{-1}: –CH_3; 2969 cm^{-1}: –C–H.

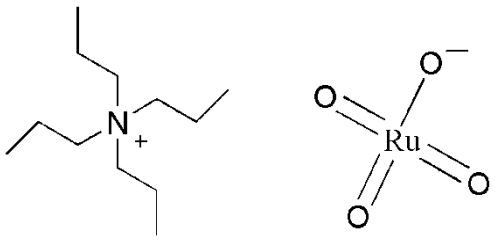

Scheme 1. The molecular formula of tetrapropylammonium perruthenate.

2.2.2. The Texture Properties of the Ru-Based Catalysts

The texture properties of the samples, including AC, Ru/AC, TPAP/AC, TPAP/AC-HNO_3, and TPAP/AC-HCl were revealed through the low-temperature N_2 adsorption–desorption experiments. All of the catalysts show the type-I adsorption/desorption isotherms (Figure S1), suggesting the large amount of micro-pores in catalysts [28].

Table 1 lists the BET (Brunauer-Emmett-Teller) specific surface areas (S_{BET}) and the total pore volumes (V_p) of each catalyst before and after the reaction. It is not difficult to find that all of the fresh samples exhibit the S_{BET} and V_p lower than those of bare AC. It ascribes to the successful loading of metallic species [6]. Through the data analysis, it is concluded that the change of the S_{BET} and V_p of TPAP/AC-HCl during the reaction is the smallest, which may be one of the reasons for its high catalytic activity and slow inactivation rate. After the 48 hours' reaction, the spent catalysts show a

lower S_{BET} and V_p than those of the associated fresh ones. The relative difference of catalysts' BET surface areas (ΔS_{BET}%) before and after the reaction decreases in the following order: TPAP/AC-HNO_3 (47.2%) > TPAP/AC (34.9%) > Ru/AC (31.7%) > AC (25.1%) > TPAP/AC-HCl (23.1%). The relative difference in the catalysts' V_p also exhibits a similar tendency. When compared with activated carbon, the S_{BETs} and V_{ps} of the Ru/AC and TPAP/AC catalysts decrease significantly, which may be caused by the metal-catalyzed reaction [29]. In addition, the initial conversions of acetylene are 40.4%, 55.8%, 78.4%, 86.0%, and 95.6% over AC, Ru/AC, TPAP/AC, TPAP/AC-HNO_3, and TPAP/AC-HCl catalysts, which decreased respectively to 7.1%, 48.3%, 69.3%, 84.8%, and 89.6% after 48 hours' reaction. Therefore, the decrease of the S_{BET}, as well as V_p, could be ascribed to the carbonaceous material deposition during the reaction or the collapse of the pores in the catalysts, resulting in a decrease in the activity of the catalysts [29].

Table 1. The texture properties of the different samples [a].

Sample	S_{BET} (m^2 g^{-1})		ΔS_{BET} (%)	V_p (cm^3 g^{-1})		ΔV_p (%)
	Fresh	Used		Fresh	Used	
AC	1237	927	25.1	0.68	0.50	26.5
Ru/AC	1160	792	31.7	0.64	0.44	31.3
TPAP/AC	962	626	34.9	0.52	0.34	34.6
TPAP/AC-HCl	1032	794	23.1	0.56	0.44	21.4
TPAP/AC-HNO_3	1013	535	47.2	0.55	0.29	47.3

[a] S_{BET}: surface area; V_p: total pore volume.

2.2.3. The Coke Deposition on the Spent Catalysts during the Reaction

The coke deposition of the spent catalyst was investigated by TGA, as shown in Figure 3. Taking TPAP/AC-HCl as an example, not only the fresh but also the spent TPAP/AC-HCl catalysts exhibit a slight mass loss before 150 °C because of the water desorption or small molecules desorption on the catalysts' surface [30]. Within the scope of 150–385 °C, there is a slowly mass loss for both the fresh and spent catalysts. However, there is a rapid mass loss for the catalysts because of the combustion of carrier when the temperature exceeds 385 °C. In consideration of that the activated carbon itself can lose its weight in air atmosphere to produce CO_2, the mass loss in the range of 150–385 °C reflects the coke deposition amount on the spent TPAP/AC-HCl catalyst [31].

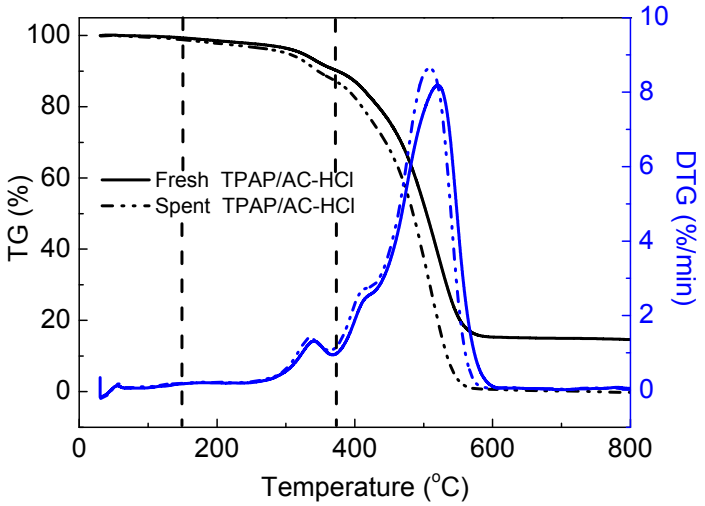

Figure 3. TG (Thermogravimetric) curves of the fresh and spent TPAP/AC-HCl catalysts.

The coke deposition amount on the other spent catalysts is also calculated by the above method [32], and is listed in Table 2. The TPAP/AC-HCl catalyst has the least coke deposition of 2.2 wt %. The coke deposition amount decreases along the following order: TPAP/AC-HNO_3 (7.3%) > TPAP/AC (4.5%) > Ru/AC (2.8%) > TPAP/AC-HCl (2.2%) (Figure S2). This result is in accord with the BET results. The substitution of the original $RuCl_3$ precursor with high valent ruthenium complex TPAP does not decrease the amount of coke deposition, however, the acidification of the carrier by hydrochloric acid is conducive to inhibit the coking deposition of TPAP catalyst to some extent.

Table 2. The amount of coke deposition on the Ru-based catalysts.

Catalysts	Amount of Carbon Deposition (%)
Ru/AC	2.8
TPAP/AC	4.5
TPAP/AC-HNO_3	7.3
TPAP/AC-HCl	2.2

2.2.4. The Dispersion of Active Species on the Catalysts

Figure 4 presents the X-ray diffraction patterns of the fresh and spent Ru/AC, TPAP/AC, TPAP/AC-HNO_3, and TPAP/AC-HCl catalysts. It can be observed that all of the fresh catalysts have two distinct diffraction peaks at 23.40° and 43.50°, which relates to the amorphous diffraction peaks of AC (Figure 4a). But beyond that, there are no characteristic Ru reflections observed, indicating that the ruthenium species are highly dispersed and that the particle size is less than 4 nm, lower than the XRD detection limit or the catalyst has a large amount of amorphous active species. After the reaction, no obvious Ru reflection could be seen but the amorphous diffraction peaks of AC (Figure 4b); it indicates that there is no obvious agglomeration or sintering of the active components during the reaction. Figure 5 presents the transmission electron microscopy (TEM) images of the carbon-supported Ru-based catalysts before and after the reaction. It can be observed that the active species are well dispersed on the catalysts, and that the particles in the fresh catalyst are tiny, uniform, and difficult to distinguish; as for the spent catalysts, there appears the agglomeration of the Ru species to some extent. For example, the average size of particles in all of the fresh catalysts is in the range of 1–3 nm, and the TPAP/AC catalyst experienced 48 hours' reaction exhibits the most serious sintering with the average particle size of 1.95 nm (Figure S3). The acidification treatment of AC in TPAP/AC catalyst can inhibit the agglomeration or sintering of the active components in the reaction process (Figure 5e–h), which is consistent with the results of X-ray diffraction (XRD) analysis.

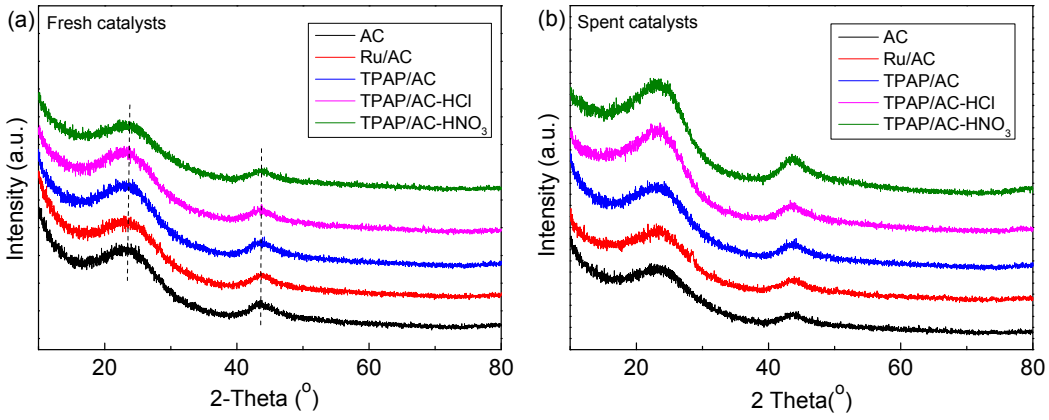

Figure 4. X-ray diffraction (XRD) patterns of the fresh (**a**) and spent (**b**) Ru-based catalysts.

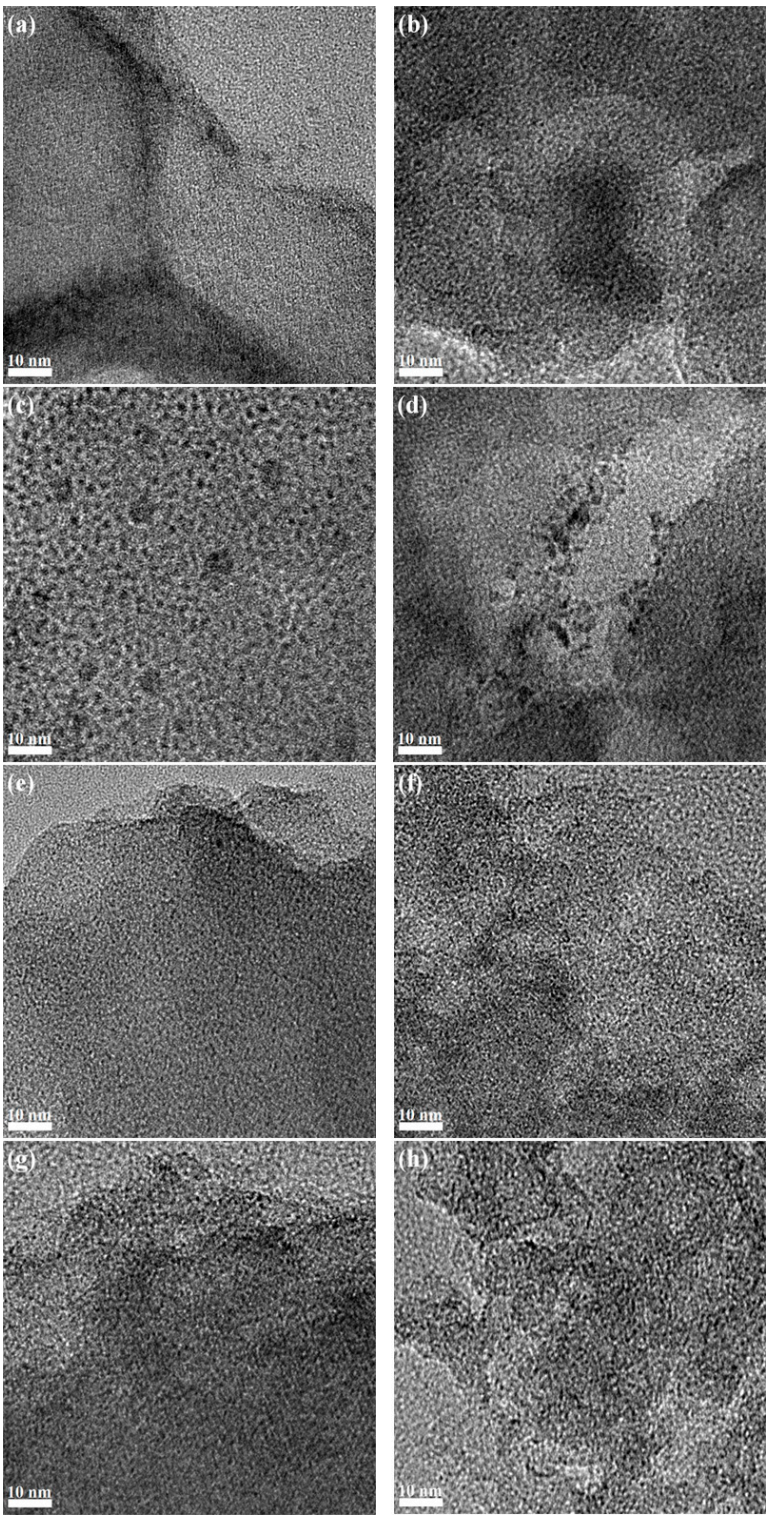

Figure 5. Transmission electron microscopy (TEM) images of the fresh and spent Ru-based catalysts: (**a**) fresh Ru/AC, (**b**) spent Ru/AC, (**c**) fresh TPAP/AC, (**d**) spent TPAP/AC, (**e**) fresh TPAP/AC-HCl, (**f**) spent TPAP/AC-HCl, (**g**) fresh TPAP/ AC-HNO, (**h**) spent TPAP/AC-HNO_3.

2.2.5. The Valence of Active Species in the Catalysts

Figure 6 presents the TPR (Temperature-programmed reduction) profiles of the prepared catalysts before and after the reaction. For all the fresh catalysts, the broad peaks appeared in 450–700 °C

associate to the characteristic reduction of oxygen-containing functional groups on AC (Figure 6) [33,34]. For the original Ru/AC catalyst, the TPR profile appears several reduction bands centered at 150.0 °C, 256.5 °C, and 325.0 °C, which are related to the reduction of RuO_x ($x > 2$), RuO_2, and $RuCl_3$, respectively (Figure 6a). The reduction temperature of Ru species in TPAP/AC decrease to 135.6 °C, 249.4 °C, and 321.7 °C for RuO_x, RuO_2, and $RuCl_3$, respectively. The TPAP/AC-HNO_3 and TPAP/AC-HCl catalysts have the TPR curves similar to the TPAP/AC catalyst, with the peak reduction temperatures transfer to lower values. These temperature shifts indicate the interactions between the carrier and ruthenium species, which in turn affects the relative content of different ruthenium species. By calculating the reduction area of TPR profiles, it can be seen that the relative amount of the ruthenium oxides in the catalyst decreases along the order: TPAP/AC-HCl > TPAP/AC-HNO_3 > TPAP/AC > Ru/AC. It shows that the substitution of $RuCl_3$ with high valent TPAP, results in more ruthenium oxides in the catalyst, and the acidification treatment of AC in TPAP catalyst can further increase the amount of active species, which is crucial to enhance the catalytic activity and stability of the prepared catalysts. In addition, the TPAP/AC-HCl has the similar amount of active ruthenium oxides to the TPAP/AC-HNO_3 catalyst for the spent catalysts, much higher than that in TPAP/AC and Ru/AC catalysts (Figure 6b).

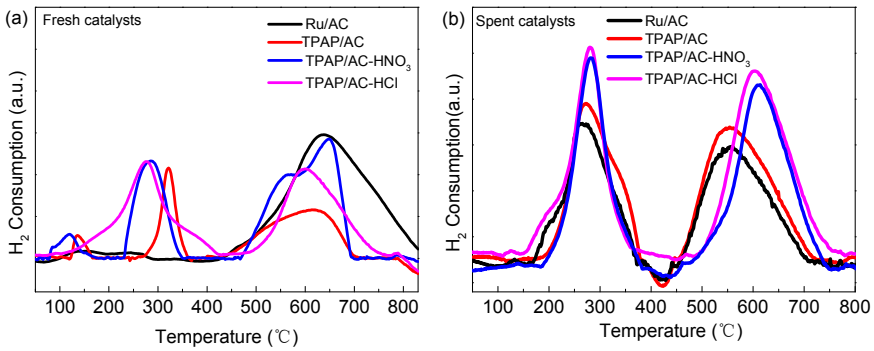

Figure 6. TPR profiles of the fresh (**a**) and spent (**b**) Ru-based catalysts.

X-ray photoelectron spectroscopy (XPS) spectra were obtained to further distinguish the different species and the relative content of them in the prepared catalysts. Since the signal of Ru3d peak coincides with that of Cls peak, the Ru 3p3/2 XPS deconvolution spectrum is adopted to distinguish the different species (Figure S4 and Table 3). For the fresh catalysts, there appear four kinds of Ru species including metallic Ru^0 at 461.6 eV, $RuCl_3$ at 463.4 eV, RuO_2 at 464.6 eV and RuO_x at 466.1 eV in the original Ru/AC catalyst [35–37], and the relative content of them is 14.0%, 49.9%, 19.1%, and 17.0%, respectively. The TPAP/AC catalyst contains 11.3% Ru^0, 42.5% $RuCl_3$, 25.1% RuO_2, and 21.1% RuO_x. The dominant species in TPAP/AC-HNO_3 is 34.5% $RuCl_3$, followed by 30.4% RuO_2, 26.2% RuO_x, and 8.9% Ru^0. The TPAP/AC-HCl catalyst contains 32.0% RuO_2, followed by 29.4% RuO_x, 20.5% $RuCl_3$, and 18.1% Ru^0. The amount of ruthenium oxides (RuO_2 and RuO_x) decreases along the following order: TPAP/AC-HCl (61.4%) > TPAP/AC-HNO_3 (56.6%) > TPAP/AC (46.2%) > Ru/AC (36.1%). It is reported that ruthenium oxides are the key active species in Ru catalysts for the reaction [28]. For the spent catalysts, the relative amount of ruthenium oxides species goes down, and that of Ru^0 species significantly increased after experiencing 48 h of reaction. It indicates that the high-valence ruthenium active species are reduced to low-valence ones during the reaction, which may result in the fall of the activity of Ru catalysts. Therefore, the substitution of $RuCl_3$ precursor with high valent TPAP species leads to more ruthenium oxides in the catalyst, and the acidification of AC in TPAP catalyst is beneficial to further improve the amount of high valence ruthenium active species in the catalysts, similar to the TPR results.

Table 3. The relative content and binding energy of ruthenium species in the fresh and spent catalysts.

Samples	Binding Energy (eV), (Area %)				Area %
	Ru	$RuCl_3$	RuO_2	RuO_x	RuO_x + RuO_2
Fresh Ru/AC	461.7 (14.0)	463.4 (49.6)	464.6 (19.0)	466.1 (17.4)	(36.4)
Fresh TPAP/AC	461.2 (11.3)	463.3 (42.5)	464.8 (25.1)	466.9 (21.1)	(46.2)
Fresh TPAP/AC-HNO_3	461.7 (8.9)	463.4 (34.5)	464.0 (30.4)	465.8 (26.2)	(56.6)
Fresh TPAP/AC-HCl	461.6 (18.1)	463.3 (20.5)	464.2 (32.0)	465.6 (29.4)	(61.4)
Used Ru/AC	461.0 (26.2)	463.0 (44.5)	465.1 (14.6)	466.5 (14.7)	(29.3)
Used TPAP/AC	461.3 (22.8)	463.5 (40.2)	464.0 (19.8)	466.8 (17.2)	(37.0)
Used TPAP/AC-HNO_3	461.7 (27.8)	462.9 (31.0)	464.0 (26.6)	466.1 (14.6)	(41.2)
Used TPAP/AC-HCl	461.6 (28.3)	463.1 (22.2)	464.1 (28.8)	465.9 (20.7)	(49.5)

2.2.6. The Adsorption Property of Ru-Based Catalysts for Reactants

C_2H_2- and HCl-TPD profiles are obtained to discuss the adsorption ability of reactants on the fresh Ru-based samples. Several desorption peaks for C_2H_2 are centered in 50–750 °C for all of the prepared catalysts (Figure 7a), which suggests the presence of the multi-status adsorbed acetylene. The peak area for C_2H_2 desorption gradually increases along the following order: Ru/AC < TPAP/AC < TPAP/AC-HNO_3 < TPAP/AC-HCl. It can be observed that the acidification of AC in TPAP catalyst is conducive to increase adsorption capacity of acetylene. Figure 7b presents the desorption peak of HCl on the prepared catalysts. In contrast, the desorption peaks are broad bands centered at ca. 400 °C for the fresh prepared samples, and the desorption areas and temperatures for HCl on the catalysts also gradually increase along the same order: Ru/AC < TPAP/AC < TPAP/AC-HNO_3 < TPAP/AC-HCl. In view of this, it can be concluded that the substitution of $RuCl_3$ with high valent TPAP species also enhances the adsorption ability of HCl, and the acidification of AC, especially by hydrochloric acid in TPAP catalyst, may produce an interaction between the carrier and the Ru species to further enhance the adsorption strength and capacity for hydrogen chloride reactant, thus increasing the activity of the resultant catalyst.

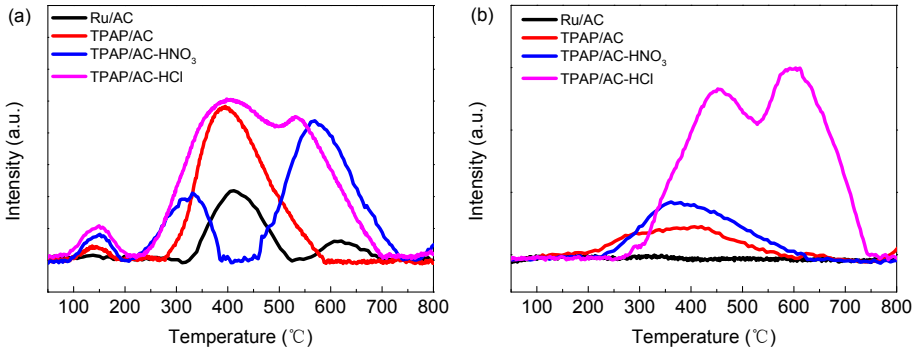

Figure 7. C_2H_2- (**a**) and HCl- (**b**) TPD profiles of the fresh Ru-based catalysts.

3. Experimental

3.1. Materials

$RuCl_3$ (Ru content ≥ 48.7%, Tianjin Fengchuan Chemical Reagent Technology Co., Ltd., Tianjin, China); nitric acid (65.0–68.0 wt %, Tianjin Fengchuan Chemical Reagent Technology Co., Ltd., Tianjin, China); Tetrapropylammonium perruthenate (TPAP, Shanghai Aladdin Biological Technology Co., Ltd., Shanghai, China); hydrochloric acid (AR, Tianjin Yongsheng Chemical Reagent Co., Ltd., Tianjin, China); coconut AC (neutral, Tangshan United Carbon Technology Co., Ltd., Tangshan, China). All the other materials can be used directly without further purification.

3.2. Acidification Pretreatment of AC

Acidification pretreatment of AC was performed according to the reported method as follows [38,39]: 5 g AC was slowly put into the 100 mL nitric acid solution (5 mol L^{-1}) at ambient temperature; the mixture was refluxed and condensed at 60 °C for 8 h; then, the resultant was filtrated and washed until the filtrate was neutral; finally the product was desiccated at 110 °C for 14 h, and termed AC-HNO_3. Similarly, the AC sample was also acidification pretreated by concentrated hydrochloric acid (12 mol L^{-1}), and the resultant was termed AC-HCl.

3.3. Preparation of the Ru-Based Catalysts

AC carrier was adopted to prepare the Ru catalysts (1 wt % Ru) via an incipient wetness impregnation method [12,29]. $RuCl_3$ aqueous solution (6.4 mL, 0.01 g mL^{-1}) was added quantitatively into AC (3 g) under constant stirring, then it was dipped for a whole day, filtered, and washed several times to reach the neutral pH value. Subsequently, the resultant sample was dried for 24 h at 140 °C to obtain the $RuCl_3$/AC catalyst. The TPAP/AC catalyst was prepared by mixing TPAP aqueous solution (10.8 mL, 0.01 g mL^{-1}) with weighed AC (3 g) under constant stirring for 24 h at room temperature and then desiccated the obtained sample at 140 °C for 24 h. A $RuCl_3$ or TPAP aqueous solution was quantitatively mixed with the hydrochloric acid or nitric acid pretreated AC according to the above procedure to prepare the Ru-based catalysts with a 1 wt % Ru loading, and the products were denoted as Ru/AC, TPAP/AC, TPAP/AC-HNO_3, and TPAP/AC-HCl, respectively.

3.4. Catalyst Characterization

Fourier transform infrared spectra (FT-IR) was acquired by a Nicolet Avatar spectrometer (Thermo Fisher Scientific, Waltham, MA, USA) to recognize the change of functional groups on the catalysts' surface. The texture property analysis was performed by a Micromeritics ASAP 2020 specific surface area and porosity analyzer (Micromeritics Instrument Ltd., Atlanta, GA, USA). Each sample was firstly degassed at 150 °C for 6 h prior to the gas adsorption/desorption at −196 °C. Thermogravimetric analysis (TGA) was conducted with a thermogravimetric differential scanning calorimetry simultaneous analyzer (NETZSCH STA449F5, NETZSCH, Selb, Germany) under an air atmosphere flow of 30 mL min^{-1}. The test temperature was set in the range of 50–800 °C with an increment of 10 °C min^{-1}. X-ray diffraction (XRD) analysis was conducted by an X'PERT PANalytical diffractometer (Bruker, Karlsruhe, Germany), using a Cu Kα radiation source operating at 40 mA and 40 kV. The patterns were recorded between 2θ values of 10°–90° with a back filled sample. Transmission electron microscopy (TEM) was performed on a G2F20 electron microscope (FEI, Hillsboro, OR, USA). The sample is firstly ground into powder and then dispersed in an ethanol solution, which is supported by a copper grid wrapped in a carbon film to acquire the analysis images. TPR experiments were carried out using a ChemBET TPR/TPD chemisorption analyser (Micromeritics Instrument Ltd., Atlanta, GA, USA) connected to a TCD. A 0.10 g sample was filled into a tube between quartz wool. The sample was then heated from 25 °C to 800 °C with an increment of 10 °C min^{-1} under a 40 mL min^{-1} 10% H_2/Ar flow. X-ray photoelectron spectroscopy (XPS) spectra were obtained using an Axis Ultra spectrometer (Shimadzu, Kyoto, Japan) equipped with a monochromatized Al Kα X-ray source; the spectral regions corresponding to the C1s core levels and Ru3p3 were recorded for the related samples. The binding energy of the species was referenced to that of C1s (284.6 eV). Temperature-programmed desorption (TPD) measurements were also performed using a ChemBET TPR/TPD chemisorption analyser (Micromeritics Instrument Ltd., Atlanta, GA, USA) connected to a TCD. The samples were placed in a reactant stream at the reaction temperature for 6 h. Then, the corresponding profiles were acquired when the temperature increased from 25 °C to 400 °C with a 10 °C min^{-1} increment and a 45 mL min^{-1} N_2 flow.

3.5. Catalytic Performance Test

The catalytic performance of the catalysts was evaluated in a fixed-bed reactor (internal diameter of 10 mm). A nitrogen purge was adopted in order to remove a small amount of moisture from the whole system. A 20 mL min^{-1} HCl (gas, 99%) flow is then introduced to activate the filled catalyst (2 mL). After the catalyst bed was heated to the reaction temperature under the atmospheric pressure, acetylene and hydrogen chloride were fed through the heated reactor, and the flow rates of the reactants were controlled via mass flow controllers to maintain a V_{HCl}/V_{C2H2} of 1.15 and a GHSV(C_2H_2) of 180 h^{-1}. The gas effluents were finally analyzed on-line using a GC-2014C gas chromatography.

4. Conclusions

A series of carbon-supported Ru-based catalysts were prepared for the hydrochlorination of acetylene, and the effects of the high valent ruthenium precursor and acidification pretreatment of the carrier on the catalytic behavior of the catalysts were also investigated. The results of catalytic performance tests indicate that the best catalytic performance is achieved over TPAP/AC-HCl catalyst with the acetylene conversion falling from 97% to 91% in 48 hours' reaction under the conditions of 180 °C, V_{HCl}/V_{C2H2} of 1.15, and a GHSV(C_2H_2) of 180 h^{-1}. The analysis results indicate that the substitution of $RuCl_3$ precursor with high valent TPAP species leads to more ruthenium oxides active species in the catalysts; the acidification treatment of carrier in TPAP/AC catalyst can produce an enhanced interaction between the active species and the modified functional groups on the carrier, which is beneficial to inhibit the carbon deposition and the sintering of active species in the reaction process, greatly increase the adsorption ability of reactants, and further increase the amount of high valent active species in the catalysts, thus improving the catalytic performance of the prepared catalysts. This also provides a promising strategy to explore high efficient and economic non-mercury catalysts for the direct synthesis of VCM.

Supplementary Materials: The following are available online at www.mdpi.com/2073-4344/7/10/311/s1, Figure S1: Nitrogen adsorption-desorption isotherms of the fresh (a) and spent (b) catalyst, Figure S2: Thermogravimetric analysis (TGA) curves of fresh and spent catalysts recorded in air atmosphere, Figure S3: Particle size distribution of Ru-based catalysts, Figure S4: High-resolution XPS spectra of Ru 3p for the fresh and spent catalysts.

Acknowledgments: This work was supported by the Start-Up Foundation for Young Scientists of Shihezi University (RCZX201507), NSFC (21706167, 21776179), the Program for Changjiang Scholars and Innovative Research Team in University (No. IRT_15R46), and Yangtze River Scholar Research Project of Shihezi University (No. CJXZ201601).

Author Contributions: Haiyang Zhang and Jinli Zhang conceived and designed the experiments; Xing Li performed the experiments; Xing Li, Baochang Man, Lijuan Hou, Chuanming Zhang and Hui Dai analyzed the data; Mingyuan Zhu, Yanzhao Dong and Bin Dai contributed reagents/materials/analysis tools; Haiyang Zhang and Xing Li wrote the paper.

Conflicts of Interest: The authors declare no conflict of interest.

References

1. Hutchings, G.J. Vapor phase hydrochlorination of acetylene: Correlation of catalytic activity of supported metal chloride catalysts. *J. Catal.* **1985**, *96*, 292–295. [CrossRef]
2. Oliver-Meseguer, J.; Doménech-Carbó, A.; Boronat, M.; Leyva-pérez, A.; Corma, A. Partial reduction and selective transfer of hydrogen chloride on catalytic gold nanoparticles. *Angew. Chem. Int. Ed.* **2017**, *56*, 6435–6439. [CrossRef] [PubMed]
3. Li, X.; Zhu, M.; Dai, B. $AuCl_3$ on polypyrrole-modified carbon nanotubes as acetylene hydrochlorination catalysts. *Appl. Catal. B Environ.* **2013**, *142–143*, 234–240. [CrossRef]
4. Wang, B.; Yu, L.; Zhang, J.; Pu, Y.; Zhang, H.; Li, W. Phosphorus-doped carbon supports enhance gold-based catalysts for acetylene hydrochlorination. *RSC Adv.* **2014**, *4*, 15877–15885. [CrossRef]
5. Conte, M.; Carley, A.F.; Hutchings, G.J. Reactivation of a carbon-supported gold catalyst for the hydrochlorination of acetylene. *Catal. Lett.* **2008**, *124*, 165–167. [CrossRef]

6. Zhang, H.; Li, W.; Li, X.; Zhao, W.; Gu, J.; Qi, X.; Dong, Y.; Dai, B.; Zhang, J. Non-mercury catalytic acetylene hydrochlorination over bimetallic Au-Ba(II)/AC catalysts. *Catal. Sci. Technol.* **2015**, *5*, 1870–1877. [CrossRef]
7. Zhou, K.; Wang, W.; Zhao, Z.; Luo, G.; Miller, J.T.; Wong, M.S.; Wei, F. Synergistic gold–bismuth catalysis for non-mercury hydrochlorination of acetylene to vinyl chloride monomer. *ACS Catal.* **2014**, *4*, 3112–3116. [CrossRef]
8. Zhao, J.; Xu, J.; Xu, J.; Ni, J.; Zhang, T.; Xu, X.; Li, X. Activated-carbon-supported gold–cesium(I) as highly effective catalysts for hydrochlorination of acetylene to vinyl chloride. *ChemPlusChem* **2014**, *80*, 196–201. [CrossRef]
9. Zhu, M.; Kang, L.; Su, Y.; Zhang, S.; Dai, B. MClx (M = Hg, Au, Ru; x = 2, 3) catalyzed hydrochlorination of acetylene-A density functional theory study. *Can. J. Chem.* **2013**, *91*, 120–125. [CrossRef]
10. Li, G.; Li, W.; Zhang, H.; Pu, Y.; Sun, M.; Zhang, J. Non-mercury catalytic acetylene hydrochlorination over Ru catalysts enhanced by carbon nanotubes. *RSC Adv.* **2015**, *5*, 9002–9008. [CrossRef]
11. Gu, J.; Gao, Y.; Zhang, J.; Li, W.; Dong, Y.; Han, Y. Hydrochlorination of acetylene catalyzed by an activated carbon-supported ammonium hexachlororuthenate complex. *Catalysts* **2017**, *7*, 17. [CrossRef]
12. Zhang, J.; Sheng, W.; Guo, C.; Li, W. Acetylene hydrochlorination over bimetallic Ru-based catalysts. *RSC Adv.* **2013**, *3*, 21062–21068. [CrossRef]
13. Shang, S.; Zhao, W.; Wang, Y.; Li, X.; Zhang, J.; Han, Y.; Li, W. Highly efficient Ru@IL/AC to substitute mercuric catalyst for acetylene hydrochlorination. *ACS Catal.* **2017**, *7*, 3510–3520. [CrossRef]
14. Man, B.; Zhang, H.; Zhang, J.; Li, X.; Xu, N.; Dai, H.; Zhu, M.; Dai, B. Oxidation modification of Ru-based catalyst for acetylene hydrochlorination. *RSC Adv.* **2017**, *7*, 23742–23750. [CrossRef]
15. Ohyama, J.; Ishikawa, H.; Mahara, Y.; Nishiyama, T.; Satsuma, A. Formation of Ru shell on Co/Al_2O_3 by galvanic deposition method and its high catalytic performance for three-way conversion. *Bull. Chem. Soc. Jpn.* **2016**, *89*, 914–921. [CrossRef]
16. Zhu, L.; Liu, X.; Jiang, H.; Sun, L. Metal-Organic frameworks for heterogeneous basic catalysis. *Chem. Rev.* **2017**, *117*, 8129–8176. [CrossRef] [PubMed]
17. Yamamoto, E.; Kuroda, K. Colloidal mesoporous silica nanoparticles. *Bull. Chem. Soc. Jpn.* **2016**, *89*, 501–539. [CrossRef]
18. Copéret, C.; Comas-Vives, A.; Conley, M.; Estes, D.; Fedorov, A.; Mougel, V.; Nagae, H.; Núñez-Zarur, F.; Zhizhko, P. Surface organometallic and coordination chemistry toward single-site heterogeneous catalysts: Strategies, methods, structures, and activities. *Chem. Rev.* **2016**, *116*, 323–421. [CrossRef] [PubMed]
19. Zhang, H.; Dai, B.; Wang, X.; Xu, L.; Zhu, M. Hydrochlorination of acetylene to vinyl chloride monomer over bimetallic Au-La/SAC catalysts. *J. Ind. Eng. Chem.* **2012**, *18*, 49–54. [CrossRef]
20. Zhao, W.; Li, W.; Zhang, J. Ru/N-AC catalyst to produce vinyl chloride from acetylene and 1, 2–dichloroethane. *Catal. Sci. Technol.* **2016**, *6*, 1402–1409. [CrossRef]
21. Xu, N.; Zhu, M.; Zhang, J.; Zhang, H. Nitrogen functional groups on an activated carbon surface to effect the ruthenium catalysts in acetylene hydrochlorination. *RSC Adv.* **2015**, *5*, 86172–86178. [CrossRef]
22. Biniak, S.; Szymański, G.; Siedlewski, J.; Tkowski, A.Ś.J. The characterization of activated carbons with oxygen and nitrogen surface groups. *Carbon* **1997**, *35*, 1799–1810. [CrossRef]
23. Hong, X.; Brown, N.M.D.; Al-Assadi, K.F.; Meenan, B.J. Surface characterization of highly oriented pyrolytic graphite modified by oxygen radio-frequency plasmas. *J. Mater. Sci. Lett.* **1993**, *12*, 201–204. [CrossRef]
24. Dandekar, A.; Baker, R.T.K.; Vannice, M.A. Characterization of activated carbon, graphitized carbon fibers and synthetic diamond powder using TPD and DRIFTS. *Carbon* **1998**, *36*, 1821–1831. [CrossRef]
25. Freivogel, P.; Grutter, M.; Forney, D.; Maier, J.P. Infrared bands of mass-selected carbon chains C*n* (*n* = 8–12) and C*n* − (*n* = 5–10, 12) in neon matrices. *Chem. Phys.* **1997**, *216*, 401–406. [CrossRef]
26. Cho, H.G.; Andrews, L. Infrared spectra of CH_2 = M(H)NC, CH_3-MNC, and η2 -M(NC)-CH_3 produced by reactions of laser-ablated group 5 metal atoms with acetonitrile. *J. Phys. Chem. A* **2010**, *114*, 5997–6006. [CrossRef] [PubMed]
27. Nyquist, R.A.; Potts, W.J. Infrared absorptions characteristic of the terminal acetylenic group (-C C-H). *Spectrochim. Acta* **1960**, *16*, 419–427. [CrossRef]
28. Pu, Y.; Zhang, J.; Yu, L.; Jin, Y.; Li, W. Active ruthenium species in acetylene hydrochlorination. *Appl. Catal. A-Gen.* **2014**, *488*, 28–36. [CrossRef]
29. Nkosi, B.; Coville, N.J.; Hutchings, G.J.; Adams, M.D.; Friedl, J.; Wagner, F.E. Hydrochlorination of acetylene using gold catalysts: A study of catalyst deactivation. *J. Catal.* **1991**, *128*, 366–377. [CrossRef]

30. Zhang, H.; Dai, B.; Wang, X.; Li, W.; Han, Y.; Gu, J.; Zhang, J. Non-mercury catalytic acetylene hydrochlorination over bimetallic Au–Co(III)/SAC catalysts for vinyl chloride monomer production. *Green Chem.* **2013**, *15*, 829–836. [CrossRef]
31. Liu, F.G.; Du, M.; Zhang, J.; Qiu, M. Electrochemical behavior of Q235 steel in saltwater saturated with carbon dioxide based on new imidazoline derivative inhibitor. *Corros. Sci.* **2009**, *51*, 102–109. [CrossRef]
32. Dumbuya, K.; Cabailh, G.; Lazzari, R.; Jupille, J.; Ringel, L.; Pistor, M.; Lytken, O.; Steinrück, H.P.; Gottfried, J.M. Evidence for an active oxygen species on Au/TiO_2 (110) model catalysts during investigation with in situ X-ray photoelectron spectroscopy. *Catal. Today* **2012**, *181*, 20–25. [CrossRef]
33. Zgolicz, P.D.; Stassi, J.P.; Yañez, M.J.; Scelza, O.A.; Miguel, S.R.D. Influence of the support and the preparation methods on the performance in citral hydrogenation of Pt-based catalysts supported on carbon nanotubes. *J. Catal.* **2012**, *290*, 37–54. [CrossRef]
34. Coloma, F.; Sepúlveda-Escribano, A.; Fierro, J.L.G.; Rodríguez-Reinoso, F. Gas phase hydrogenation of crotonaldehyde over Pt/activated carbon catalysts. Influence of the oxygen surface groups on the support. *Appl. Catal. A-Gen.* **1997**, *150*, 165–183. [CrossRef]
35. Zhang, H.; Li, W.; Jin, Y.; Sheng, W.; Hu, M.; Wang, X.; Zhang, J. Ru-Co(III)-Cu(II)/SAC catalyst for acetylene hydrochlorination. *Appl. Catal. B Environ.* **2016**, *189*, 56–64. [CrossRef]
36. Ma, J.; Feng, Y.; Yu, J.; Zhao, D.; Wang, A.; Xu, B. Promotion by hydrous ruthenium oxide of platinum for methanol electro-oxidation. *J. Catal.* **2010**, *275*, 34–44. [CrossRef]
37. Sharma, S.; Hu, Z.; Zhang, P.; Mcfarland, E.W.; Metiu, H. CO_2 methanation on Ru-doped ceria. *J. Catal.* **2011**, *278*, 297–309. [CrossRef]
38. Cao, H.; Xing, L.; Wu, G.; Xie, Y.; Shi, S.; Zhang, Y.; Minakata, D.; Crittenden, J.C. Promoting effect of nitration modification on activated carbon in the catalytic ozonation of oxalic acid. *Appl. Catal. B Environ.* **2014**, *146*, 169–176. [CrossRef]
39. Conte, M.; Davies, C.J.; Morgan, D.J.; Davies, T.E.; Carley, A.F.; Johnston, P.; Hutchings, G.J. Modifications of the metal and support during the deactivation and regeneration of Au/C catalysts for the hydrochlorination of acetylene. *Catal. Sci. Technol.* **2013**, *3*, 128–134. [CrossRef]